machines

MDPI

Article

Uncertainty and Sensitivity Analyses of an Annular Thermoelectric Refrigerator Based on Latin Hypercube Sampling

Jinhao Ma [1], Meilin Song [2], Xue Li [1] and Feng Zhang [1,*]

[1] School of Mechanics and Transportation Engineering, Northwestern Polytechnical University, Xi'an 710129, China
[2] Honors College, Northwestern Polytechnical University, Xi'an 710129, China
* Correspondence: nwpuwindy@nwpu.edu.cn

Abstract

Thermoelectric refrigeration systems employing the Peltier effect are widely applied in electronic cooling and environmental control. The performance of such systems is influenced by inevitable uncertainties in key parameters that can lead to noticeable variations in system responses. However, previous sensitivity analyses have been limited to flat-plate thermoelectric systems; annular thermoelectric refrigeration systems have not been analyzed. Accordingly, this study conducted a dispersion analysis of an annular thermoelectric refrigeration system by treating the input parameters as random variables that follow normal distributions and generating samples using Latin hypercube sampling. The changes in three response indicators—the cold-end temperature, refrigeration efficiency, and exergy efficiency—with small shifts in the mean and standard deviation of each input parameter were subsequently calculated to determine their influence on system performance. The results indicated that a slight decrease in the hot-side temperature significantly enhanced overall system performance, with an average influence weight of 0.45, and a moderate increase in the cold-side heat absorption improved both the refrigeration and exergy efficiencies, with an average influence weight of 0.29; by contrast, changes in the annular geometric parameter had relatively weak effects on system performance and the dispersion of system responses, exhibiting an average influence weight of only 0.02. Therefore, this study demonstrated an effective approach for evaluating the uncertainty inherent in annular thermoelectric refrigeration systems and provides a reference for optimizing their designs to ensure reliability.

Keywords: annular thermoelectric cooler; uncertainty analysis; Latin hypercube sampling; sensitivity analysis

Check for updates

Academic Editors: Matija Hoić, Mario Hrgetić and Branimir Škugor

Received: 27 April 2026
Revised: 22 May 2026
Accepted: 31 May 2026
Published: 4 June 2026

Copyright: © 2026 by the authors. Licensee MDPI, Basel, Switzerland. This article is an open access article distributed under the terms and conditions of the Creative Commons Attribution (CC BY) license.

1. Introduction

Thermoelectric refrigeration technology enables direct solid-state conversion between electrical and thermal energy [1–3]. The advantageous lack of mechanical movement, silent operation, compact size, and precise temperature control provided by thermoelectric refrigeration have led to its widespread application in fields such as the thermal regulation of medical devices [4] and LiDAR systems, as well as small-scale vehicle refrigeration [5]. Furthermore, its ability to provide accurate thermal management for power batteries can extend battery life and ensure the safe operation of new energy vehicles. However, conventional thermoelectric refrigeration systems exhibit low energy conversion efficiencies, rarely exceeding 10% [6]. This poor efficiency can primarily be attributed to the inherent

limitations of thermoelectric technology, such as Joule heat loss in thermoelectric materials and irreversible heat conduction [7,8].

Research on improving the performance of thermoelectric refrigerators has focused on two approaches. The first approach seeks to develop new thermoelectric materials with higher performance indices. For example, Yang et al. [9] achieved a high figure of merit of 1.4 at 375 K using BiSbTe composite materials, Kim et al. [10] improved the figure of merit for GeTe by doping it with Al, Xie et al. [11] employed nanocrystalline porous materials to improve device performance, and Wang et al. [12] applied high-pressure torsion to Bi_2Te_3 powders to enhance their material performance. Furthermore, Ji et al. [13] suggested that reducing the lattice thermal conductivity could effectively increase the figure of merit for thermoelectric devices, and Ali et al. [14] improved thermoelectric performance by employing In_2SSeTe materials.

The second approach focuses on optimizing the thermoelectric device structure and geometry. For example, Liu et al. [15] developed and implemented a novel three-dimensional thermoelectric cooler model incorporating ten different leg geometries, and Gao et al. [16] adopted a honeycomb structure to enhance thermoelectric performance. In addition, Zhang et al. [17] designed a novel sandwich structure that simultaneously achieved a high power output, a high coefficient of performance, and a compact size; Tsai et al. [18] introduced a herringbone-like device structure that realized excellent thermoelectric performance.

Although improving the materials and structures applied in thermoelectric refrigerators can boost cooling performance, the actual cooling effect consistently depends on the balance between the heat absorption capacity on the cold side and the heat dissipation capacity on the hot side. This balance is influenced by multiple parameters, including the structural characteristics, material properties, and operating conditions of the device. However, most previous studies employed fixed values for these parameters and rarely considered the random uncertainties present in actual engineering applications, thereby likely underestimating the effects of parameter changes on cooling performance. Furthermore, only a few uncertainty studies have been conducted on thermoelectric devices, most of which have focused on flat-plate systems. For example, Zhang et al. [19,20] analyzed the failure probabilities of various multistage thermoelectric generators using Latin hypercube sampling, and Wang et al. [21] conducted a variance-based sensitivity analysis of a thermoelectric generator using fuzzy and stochastic theories. Overall, studies investigating the effects of uncertainty on the performance of annular thermoelectric refrigeration systems, which are designed to meet the refrigeration requirements of annular spaces, remain limited.

Therefore, this study established a one-dimensional steady-state model of an annular thermoelectric refrigeration system based on existing research, then employed Latin hypercube sampling to perform a dispersion analysis, yielding the uncertainty distributions of the different considered input and response parameters. A sensitivity analysis was subsequently combined with normalization processing to investigate the responses of three system performance parameters (the cold-end temperature, refrigeration efficiency, and exergy efficiency) to variations in the input parameter uncertainty distributions. The results provide theoretical guidance and data support for the structural parameter optimization, operating condition regulation, and reliable engineering design of annular thermoelectric refrigerators.

2. Numerical Model of the Annular Thermoelectric Refrigerator

2.1. Working Principle

The core structure of an annular thermoelectric refrigerator consists of p- and n-type semiconductor elements sandwiched between a heat source and a heat sink to achieve

cooling by directly converting electrical energy into thermal energy through the Peltier effect. The general structure of an annular thermoelectric refrigerator is shown in Figure 1, where r_1 represents the radial distance from the center to the cold side and r_2 denotes the radial distance from the center to the hot side.

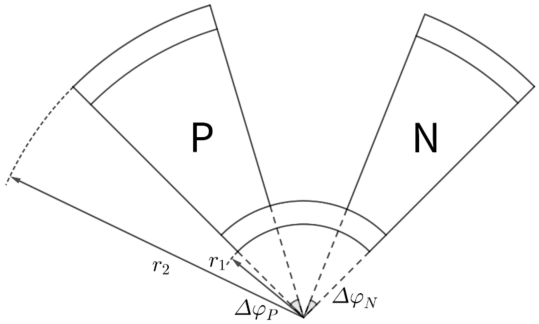


Figure 1. General structure of an annular thermoelectric refrigerator.

When direct current passes through the p–n semiconductor circuit, directional heat absorption and release occur at the junctions where the semiconductors contact the cold and hot sides. Thus, heat is absorbed on the cold side to produce a cooling effect and released on the hot side to complete the thermal cycle. The following assumptions were made in this study based on conventional thermodynamic analysis methods and practical engineering considerations to simplify the resulting theoretical model:

(1) The physical properties of the semiconductor materials, including the Seebeck coefficient, thermal conductivity, and electrical resistivity, were assumed to be constant and independent of the temperature and spatial position, so the Thomson effect was neglected [22].
(2) Only steady-state refrigeration conditions were considered.
(3) The lateral surfaces of the refrigeration system were assumed to be adiabatic, and only one-dimensional steady-state radial heat transfer was considered with heat flowing along the radial direction from the cold side to the hot side.
(4) The thermal conductivities and electrical resistivities of the p- and n-type semiconductors were considered equal to each other and equivalent to those of the complete device; the Seebeck coefficient for the p-type semiconductor was assumed to be positive, that for the n-type semiconductor was assumed to be negative, and both were set to half of that for the complete device to ensure structural and performance symmetry [23].

It should be noted that the present model is established based on a simplified theoretical framework reported in previous studies. Therefore, its applicability may vary under different engineering conditions, and further modifications may be required for specific practical applications.

2.2. Evaluation of Refrigeration Performance

The performance of the considered annular thermoelectric refrigerator was quantified by conducting energy and exergy analyses based on previous studies [19]. The cold-side temperature, refrigeration efficiency, and exergy efficiency were selected as the performance evaluation indicators for this analysis [24] and were modeled by applying the heat transfer equations with nondimensional transformations.

The laws of energy conservation and thermoelectric conversion theory were considered to express the heat transfer equations for heat absorption on the cold side per unit time (Q_c) and heat release on the hot side per unit time (Q_h) as follows:

$$Q_c = \alpha I T_c - K(T_h - T_c) - \frac{1}{2} I^2 R, \tag{1}$$

$$Q_h = \alpha I T_h - K(T_h - T_c) + \frac{1}{2} I^2 R, \tag{2}$$

where T_c denotes the cold-side temperature, T_h denotes the hot-side temperature, α denotes the Seebeck coefficient of the device, K denotes the thermal conductivity of the device, I denotes the applied current, and R denotes the electrical resistance of the device.

The influences of the annular geometry on R and K were characterized using dimensionless expressions based on the annular parameter ($S_r = r_1/r_2$) [25], as follows:

$$\frac{R}{R_0} = \frac{(S_r + 1) ln(S_r)}{S_r - 1}, \tag{3}$$

$$\frac{K}{K_0} = \frac{4(S_r - 1)}{ln(S_r)(S_r + 1)}, \tag{4}$$

where the referenced thermal conductance K_0 and electrical resistance R_0 are based on the position r_0, $r_0 = (r_1 + r_2)/2$.

The value of T_c was used as a performance indicator because it limits the refrigeration capacity of the device; it was determined by

$$T_c = \frac{(S_r + 1) Q_c ln(S_r) + 4K_0 T_h (S_r - 1)}{2K_0 \left(1 + \sqrt{1 + 4ZT_m}\right)(S_r - 1)}, \tag{5}$$

where ZT_m denotes the figure of merit for the device.

The refrigeration efficiency (η) performance indicator was defined as the ratio of the cooling capacity at the cold side to the input electrical power, as follows:

$$\eta = \frac{(S_r + 1) Q_c ln(S_r) + 4K_0 T_h (S_r - 1)}{2K_0 \left(1 + \sqrt{1 + 4ZT_m}\right)(S_r - 1)}. \tag{6}$$

The exergy efficiency (ψ) performance indicator, which reflects the energy utilization efficiency of the device, was defined as the ratio of the exergy output on the cold side to the input electrical power [26,27], as follows:

$$\psi = \frac{Q_c}{P_{in}} \left(\frac{T_h}{T_c} - 1 \right), \tag{7}$$

where P_{in} is the input electrical power.

Assuming $P_{in} = Q_h - Q_c$, Equation (7) can be reformulated to obtain [28]

$$\psi = \frac{\left(1 + \sqrt{1 + 4ZT_m}\right)^2 (S_r + 1) ln(S_r) \left(- \frac{(S_r + 1) Q_c \left(1 + 4ZT_m + \sqrt{1 + 4ZT_m}\right) \ln(S_r)}{8} + ZT_m \sqrt{1 + 4ZT_m} \, (S_r - 1) K_0 T_h \right) Q_c}{32 ZT_m \left(\frac{(S_r + 1) Q_c \ln(S_r)}{4} + K_0 T_h (S_r - 1) \right) (S_r - 1) K_0 T_h \left(\left(\sqrt{1 + 4ZT_m} + 2 \right) ZT_m + \frac{\sqrt{1 + 4ZT_m}}{2} + \frac{1}{2} \right)}. \tag{8}$$

3. Dispersion Analysis Based on Latin Hypercube Sampling

The performance of an annular thermoelectric refrigerator generally exhibits significant uncertainty according to the variations in its multiple input parameters. Therefore, the influences of input parameter uncertainties on the model-output performance parameters were evaluated using the Latin hypercube sampling (LHS) method to sample the parameter space. This method divides the probability distribution of each random input parameter into several subintervals with equal probabilities, then randomly draws a sample from each. These samples are subsequently randomly combined to form a multidimensional sample matrix, thereby ensuring a uniform distribution of samples throughout the entire parameter space [29–31].

Notably, LHS provides a higher sampling efficiency and better spatial coverage than the traditional Monte Carlo method when obtaining the same number of samples [32], effectively reducing the estimation variance. The samples generated in this study were substituted into the numerical device model derived in Section 2 to obtain the statistical characteristics of the output performance parameters and thereby facilitate the subsequent uncertainty propagation analysis. The LHS-based dispersion analysis procedure applied in this study comprised the five steps shown in Figure 2 and described in the remainder of this section. All numerical calculations and data visualization associated with the LHS analysis were performed using Python 3.11.

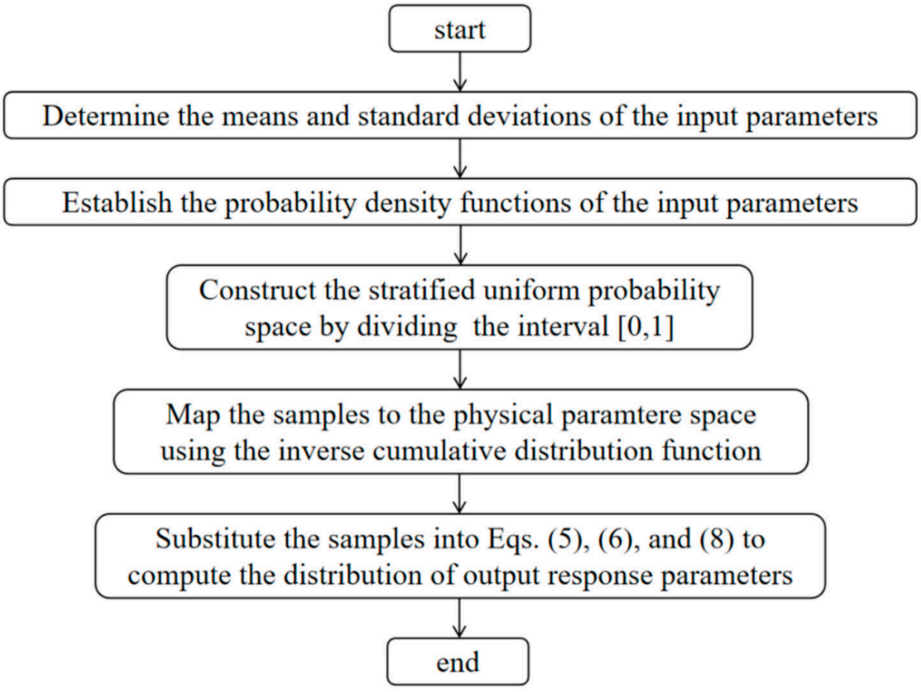


Figure 2. Flowchart of the LHS analysis.

Step 1: Determine the means and standard deviations of the input parameters.

According to Equations (5), (6), and (8), the performance of an annular thermoelectric refrigerator is affected by S_r, T_h, ZT_m, Q_c, and K_0. The uncertainties of these input parameters were captured by representing them as random variables that follow normal distributions. The means and standard deviations of these distributions were determined based on Ref. [24] and engineering experience and are presented in Table 1.

Table 1. Normal distribution parameters of the input parameters.

Parameter	Mean	Standard Deviation
S_r	0.6	0.03
T_h	300	5
ZT_m	0.6018	0.03
Q_c	0.75	0.0375
K_0	0.05	0.0025

Step 2: Establish the probability density functions for the input parameters.

The probability density function for a random variable $X_i \sim \mathcal{N}(\mu_i, \sigma_i^2)$ was determined as follows:

$$f_{X_i}(x) = \frac{1}{\sigma_i\sqrt{2\pi}}\exp\left[-\frac{(x-\mu_i)^2}{2\sigma_i^2}\right], \quad (9)$$

where μ_i denotes the mean and σ_i denotes the standard deviation for input parameter i, and x denotes the value of the random variable X_i.

The probability density functions of the input parameters S_r, T_h, ZT_m, Q_c, and K_0 were constructed in this study using the values reported in Table 1.

Step 3: Construct the stratified uniform probability space.

The stratified uniform probability space was constructed by dividing the interval $[0, 1]$ into N subintervals with equal probability as follows:

$$\left[\frac{0}{N}, \frac{1}{N}\right], \left[\frac{1}{N}, \frac{2}{N}\right], \ldots, \left[\frac{N-1}{N}, 1\right], \tag{10}$$

and then selecting a random point within each subinterval to obtain uniformly distributed samples in each subinterval from throughout the probability space.

Correlations among input parameters were eliminated by independently and randomly permuting the samples in each dimension, resulting in an LHS matrix given by:

$$U = u_{ij}, \tag{11}$$

where i denotes the input parameter and j denotes the sample.

Step 4: Map the samples to the physical parameter space.

The uniformly distributed samples were mapped onto the physical parameter space using the inverse cumulative distribution function of the target distribution, given by

$$X_{ij} = \phi^{-1}(u_{ij}; \mu_i, \sigma_i), \tag{12}$$

to obtain the sample matrix of input parameters required for the subsequent calculations.

Step 5: Calculate the distributions of response parameters.

The generated random input samples were substituted into the numerical model defined by Equations (5), (6), and (8), then the corresponding response parameters (T_c, η, and ψ) were calculated for each sample. The distributions of these response parameters are shown in Figure 3, in which the vertical axis represents the probability density, reflecting the relative likelihood of a sample occurring within a unit interval of the given parameter. It can be observed that all three response variables exhibit a certain degree of dispersion, indicating that the uncertainty in input parameters leads to noticeable variability in the system performance. Note that the area of each histogram was normalized to unity, allowing the distributions to be interpreted as probability density functions and facilitating a consistent comparison of their statistical characteristics.

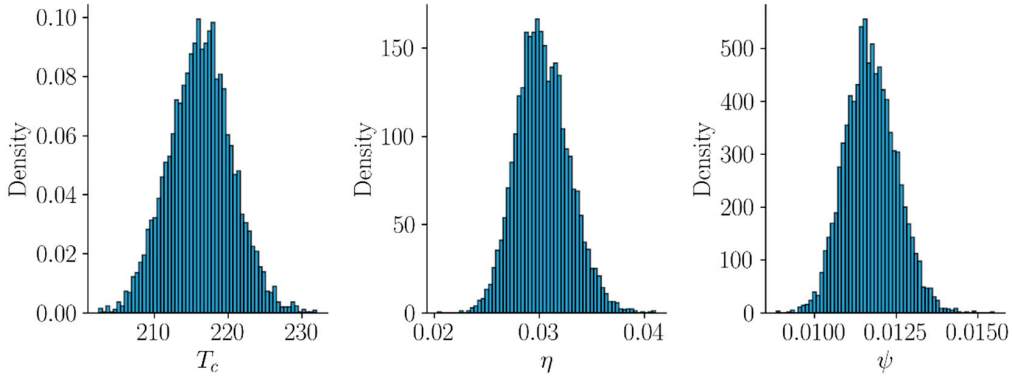


Figure 3. Probability density histograms of the response parameters.

4. Sensitivity Analysis

The sensitivity analysis represents a valuable method for evaluating the influences of input parameter variations on model outputs to identify key controlling variables and

quantify the contribution of each parameter to system performance [33]. This study systematically investigated the effects of input parameter uncertainty on the model responses in terms of T_c, η, and ψ. The sensitivity analysis applied to do so independently shifted the means and standard deviations of each input parameter distribution; its influence on the system performance was reflected by the output parameter dispersions.

4.1. Mean Shift Analysis

The mean shift analysis changed the mean value of a selected input parameter by a certain percentage while keeping its standard deviation and the remaining parameter distributions unchanged. The modified parameter distribution was subsequently substituted into the numerical model for recalculation to determine the resulting variation in the mean response parameters.

Letting μ_0 denote the baseline mean value of an input parameter X, the shifted mean value can be expressed as

$$\mu(X) = \mu_0(1+\beta),\ \beta \in [-0.1,\ 0.1], \tag{13}$$

where β represents the relative shift; in this study, the shift applied to the mean value for each input parameter was consistently varied in increments of 2% within ±10% of the original value.

The shifted values were applied in Equations (5), (6), and (8) to determine the resulting magnitude of change in each output performance parameter and thereby determine the sensitivity index as follows:

$$S_i = \frac{max(Y_i) - min(Y_i)}{Y_0}, \tag{14}$$

where S_i denotes the sensitivity index for input parameter i, Y_i represents the output parameter value obtained after that input parameter was shifted, and Y_0 denotes the output parameter value under the baseline condition.

The S_i values were subsequently normalized to obtain the weight coefficient W_i for each input parameter as follows:

$$W_i = \frac{S_i}{\sum_{i=1}^{5} S_i}, \tag{15}$$

such that the W_i of all input parameters for each output parameter satisfied:

$$\sum W_i = 1. \tag{16}$$

4.1.1. Sensitivity of Output $\mu(T_c)$

As presented in Figure 4 and Table 2, the sensitivity of the output $\mu(T_c)$ to the different input parameters varied significantly. The shift in $\mu(T_h)$ exerted the most pronounced effect on $\mu(T_c)$ (W_i = 0.776), which increased with increasing $\mu(T_h)$, indicating that the temperature difference across the system was strongly controlled by T_h. Physically, an increase in T_h weakens the heat rejection capability of the system, leading to a rise in the overall temperature level of the device. In the annular thermoelectric configuration, heat is mainly transferred along the radial direction, causing the hot-side boundary condition to strongly influence the entire temperature field. Consequently, the cold-end temperature exhibits high sensitivity to variations in hot-side temperature. The value of $\mu(ZT_m)$ had the second greatest influence on $\mu(T_c)$ (W_i = 0.183), which decreased with increasing $\mu(ZT_m)$. By contrast, the values of $\mu(Q_c)$, $\mu(K_0)$, and $\mu(S_r)$ had relatively weak effects on $\mu(T_c)$, with all three parameters showing W_i values below 0.02 and the corresponding curves exhibiting only slight variations.

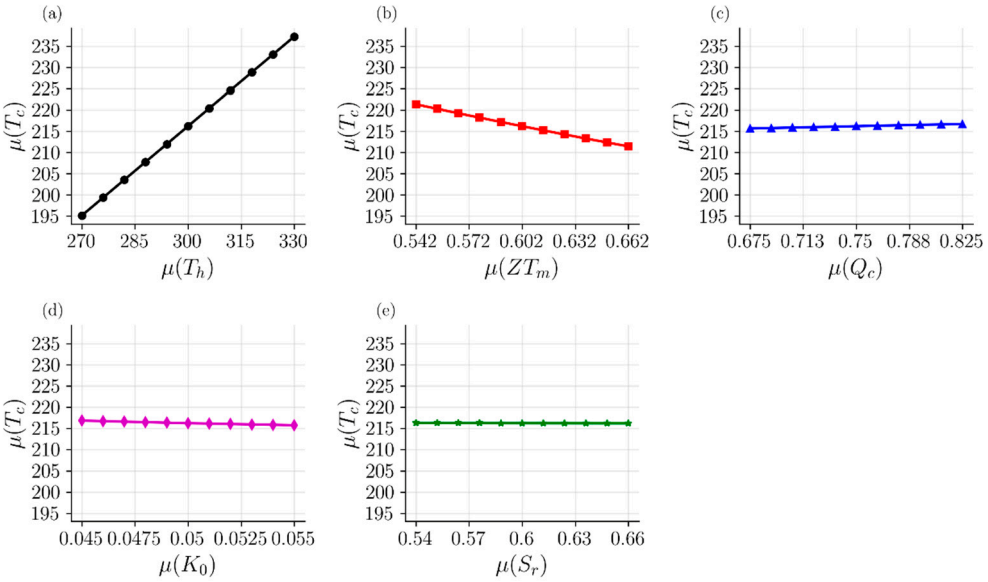


Figure 4. Variation in $\mu(T_c)$ with shifted **(a)** $\mu(T_h)$, **(b)** $\mu(ZT_m)$, **(c)** $\mu(Q_c)$, **(d)** $\mu(K_0)$, and **(e)** $\mu(S_r)$.

Table 2. Sensitivity of $\mu(T_c)$ to changes in the mean input parameters.

Shifted Input Parameter	S_i	W_i	Direction of Influence
$\mu(T_h)$	0.195	0.776	Positive
$\mu(ZT_m)$	0.046	0.183	Negative
$\mu(Q_c)$	0.005	0.020	Positive
$\mu(K_0)$	0.005	0.020	Negative
$\mu(S_r)$	0.001	0.001	Negative

4.1.2. Sensitivity of $\mu(\eta)$

Figure 5 and Table 3 illustrate the responses of $\mu(\eta)$ to shifts in the mean values of the input parameters. The $\mu(T_h)$, $\mu(Q_c)$, and $\mu(K_0)$ values all had significant effects on $\mu(\eta)$ (W_i = ~0.26), whereas $\mu(ZT_m)$ had a slightly smaller effect (W_i = 0.20), and $\mu(S_r)$ exhibited the least effect (W_i = ~0.02), presenting a nearly flat curve.

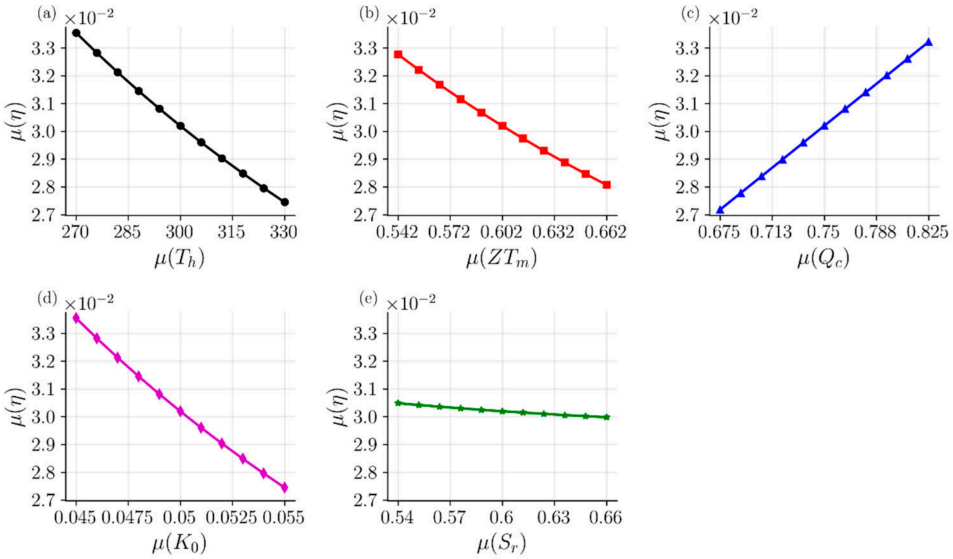


Figure 5. Variation in $\mu(\eta)$ with shifted **(a)** $\mu(T_h)$, **(b)** $\mu(ZT_m)$, **(c)** $\mu(Q_c)$, **(d)** $\mu(K_0)$, and **(e)** $\mu(S_r)$.

Table 3. Sensitivity of $\mu(\eta)$ to changes in the mean input parameters.

Shifted Input Parameter	S_i	W_i	Direction of Influence
$\mu(T_h)$	0.202	0.260	Negative
$\mu(ZT_m)$	0.156	0.200	Negative
$\mu(Q_c)$	0.200	0.258	Positive
$\mu(K_0)$	0.202	0.260	Negative
$\mu(S_r)$	0.017	0.022	Negative

4.1.3. Sensitivity of $\mu(\psi)$

Figure 6 and Table 4 present the responses of $\mu(\psi)$ to shifts in the mean input parameters. The variations in $\mu(\psi)$ with the shifts in the mean input parameters were generally similar to those in $\mu(\eta)$; however, $\mu(\psi)$ was less sensitive to changes in $\mu(ZT_m)$, and all of the S_i values were slightly smaller (by approximately 0.02), indicating that $\mu(\psi)$ was less sensitive to variations in the mean input parameters than $\mu(\eta)$.

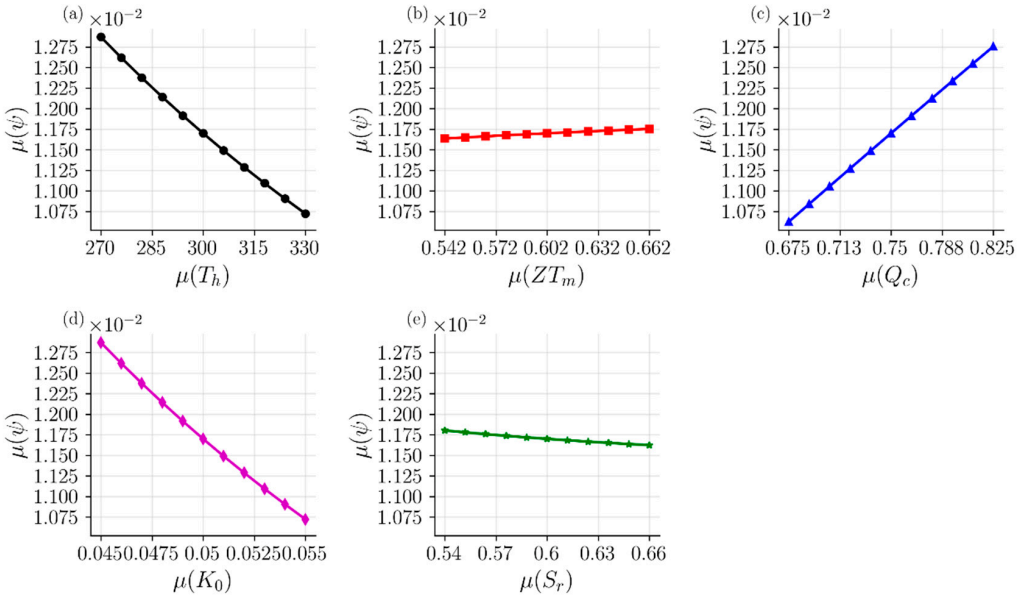


Figure 6. Variation in $\mu(\psi)$ with shifted (**a**) $\mu(T_h)$, (**b**) $\mu(ZT_m)$, (**c**) $\mu(Q_c)$, (**d**) $\mu(K_0)$, and (**e**) $\mu(S_r)$.

Table 4. Sensitivity of $\mu(\psi)$ to changes in the mean input parameters.

Shifted Input Parameter	S_i	W_i	Direction of Influence
$\mu(T_h)$	0.184	0.320	Negative
$\mu(ZT_m)$	0.010	0.017	Positive
$\mu(Q_c)$	0.182	0.317	Positive
$\mu(K_0)$	0.184	0.320	Negative
$\mu(S_r)$	0.015	0.026	Negative

4.2. Standard Deviation Shift Analysis

The influence of input parameter uncertainty on the dispersion of the system responses was analyzed by shifting the standard deviation of each random variable while keeping its mean value and the distributions for the other parameters unchanged.

Letting σ_0 denote the baseline standard deviation of an input parameter X, the shifted standard deviation can be expressed as

$$\sigma(X) = \sigma_0(1+\gamma), \gamma \in [-0.1, 0.1], \quad (17)$$

where γ represents the standard deviation shift coefficient; in this study, the shift applied to the standard deviation for each input parameter was consistently varied in increments of 2% within $\pm$10% of the original value.

The LHS process was performed after applying different standard deviation shifts to each input parameter to calculate the statistical characteristics of the output performance parameters and thereby evaluate the influence of variations in the uncertainty of the input on the dispersions of the output.

4.2.1. Sensitivity of $\sigma(T_c)$

As shown in Figure 7, variations in the standard deviations of different input parameters had different effects on $\sigma(T_c)$. The value of $\sigma(T_c)$ increased significantly with increasing $\sigma(T_h)$; it also increased with increasing $\sigma(ZT_m)$, although the magnitude of this change was relatively small. By contrast, variations in $\sigma(Q_c)$, $\sigma(K_0)$, and $\sigma(S_r)$ had weaker effects on $\sigma(T_c)$, with the corresponding curves exhibiting only minor fluctuations; overall, changes in the uncertainties of these parameters had limited influence on the dispersion of T_c.

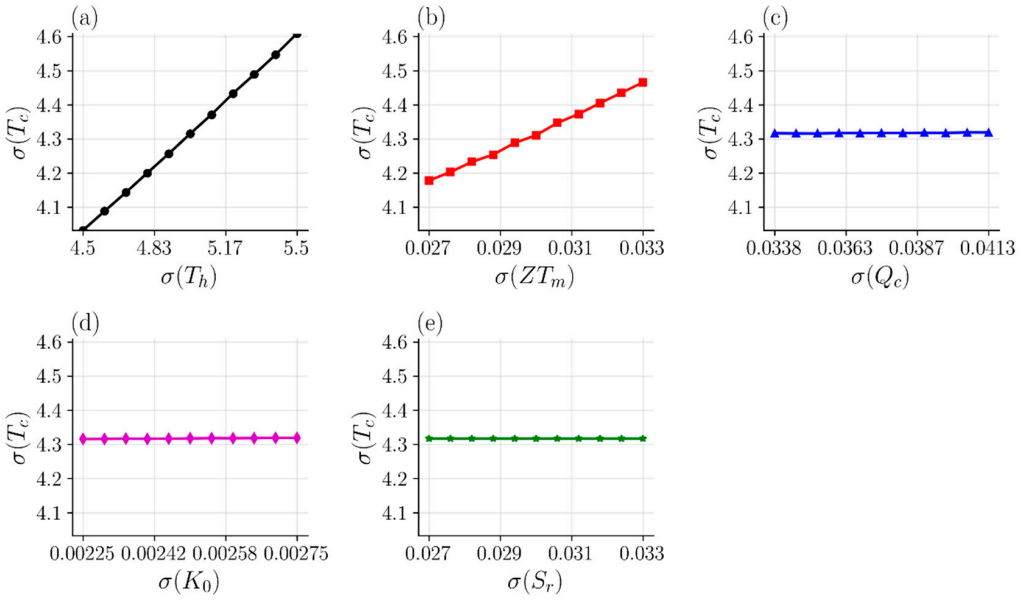


Figure 7. Variation in $\sigma(T_c)$ with shifted (**a**) $\sigma(T_h)$, (**b**) $\sigma(ZT_m)$, (**c**) $\sigma(Q_c)$, (**d**) $\sigma(K_0)$, and (**e**) $\sigma(S_r)$.

4.2.2. Sensitivity of $\sigma(\eta)$

As shown in Figure 8, an increase in $\sigma(T_h)$ only slightly increased $\sigma(\eta)$, indicating that uncertainty in T_h has a limited effect on the fluctuation of η. By contrast, increases in $\sigma(ZT_m)$, $\sigma(Q_c)$, and $\sigma(K_0)$ caused noticeable increases in $\sigma(\eta)$. However, changes in $\sigma(S_r)$ had little effect on $\sigma(\eta)$, which remained essentially stable with only minor fluctuations.

4.2.3. Sensitivity of $\sigma(\psi)$

As shown in Figure 9, shifts in $\sigma(Q_c)$ and $\sigma(K_0)$ had significant impacts on the uncertainty expressed by $\sigma(\psi)$. An increase in $\sigma(T_h)$ only slightly increased $\sigma(\psi)$, which exhibited a relatively small overall variation, indicating that the uncertainty in T_h had a limited effect on fluctuations in ψ. By contrast, changes in $\sigma(ZT_m)$ and $\sigma(S_r)$ had essentially no effect on $\sigma(\psi)$.

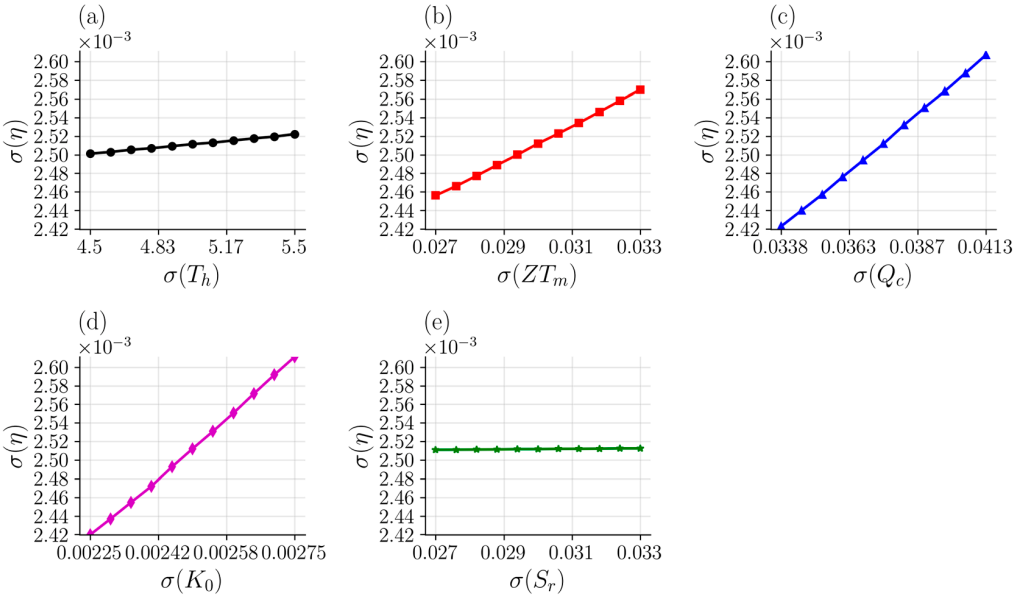


Figure 8. Variation in $\sigma(\eta)$ with shifted **(a)** $\sigma(T_{\mathrm{h}})$, **(b)** $\sigma(ZT_{\mathrm{m}})$, **(c)** $\sigma(Q_{\mathrm{c}})$, **(d)** $\sigma(K_0)$, and **(e)** $\sigma(S_{\mathrm{r}})$.

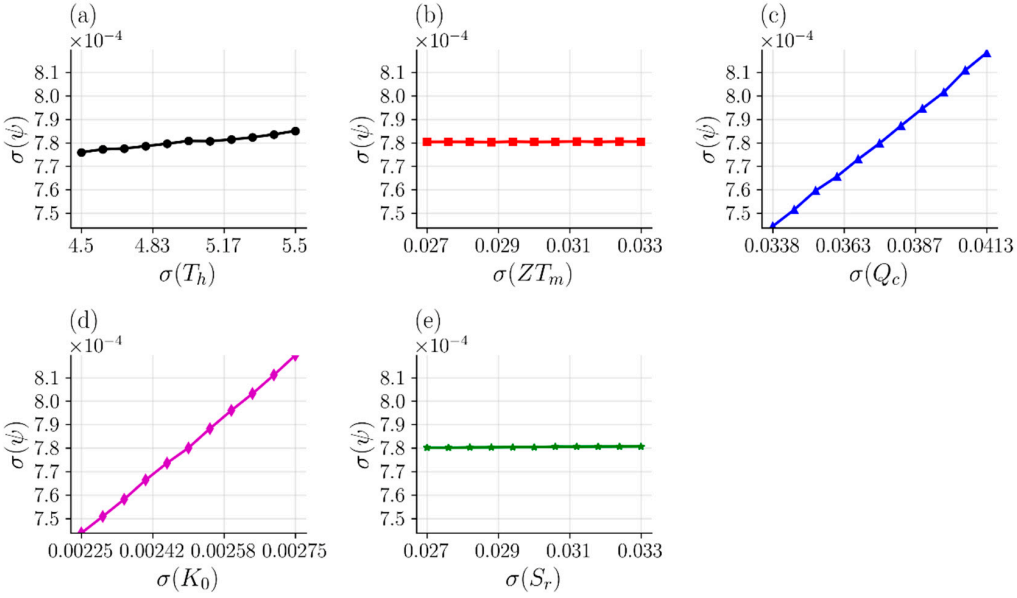


Figure 9. Variation in $\sigma(\psi)$ with shifted **(a)** $\sigma(T_{\mathrm{h}})$, **(b)** $\sigma(ZT_{\mathrm{m}})$, **(c)** $\sigma(Q_{\mathrm{c}})$, **(d)** $\sigma(K_0)$, and **(e)** $\sigma(S_{\mathrm{r}})$.

5. Conclusions

This study evaluated the effects of uncertainty in the input parameters of an annular thermoelectric cooler on its performance using an LHS-based stochastic analysis model to conduct a sensitivity analysis. The output T_{c}, η, and ψ of the thermoelectric cooling device were found to exhibit significant random dispersions. The sensitivity analysis independently shifted the mean and standard deviation of each input parameter to determine the effects on the corresponding means and standard deviations of T_{c}, η, and ψ. The results of the mean shift analysis indicated that an increase in $\mu(T_{\mathrm{h}})$ or decrease in $\mu(ZT_{\mathrm{m}})$ increased $\mu(T_{\mathrm{c}})$; a decrease in $\mu(T_{\mathrm{h}})$, decrease in $\mu(ZT_{\mathrm{m}})$, increase in $\mu(Q_{\mathrm{c}})$, or decrease in $\mu(K_0)$ all increased $\mu(\eta)$; and $\mu(ZT_{\mathrm{m}})$ had a negligible effect on $\mu(\psi)$. The results of the standard deviation shift analysis indicated that $\sigma(T_{\mathrm{h}})$ and $\sigma(ZT_{\mathrm{m}})$ significantly affected $\sigma(T_{\mathrm{c}})$; $\sigma(ZT_{\mathrm{m}})$, $\sigma(Q_{\mathrm{c}})$, and $\sigma(K_0)$ were all major contributors to the uncertainty expressed by $\sigma(\eta)$; and $\sigma(ZT_{\mathrm{m}})$ exhibited a relatively weak influence on the uncertainty expressed by $\sigma(\psi)$. Critically, variations in the mean and standard deviation of S_{r} had little effect on

any aspect of the overall system performance. These findings may provide useful guidance for the practical design and operation of annular thermoelectric refrigeration systems. For example, to achieve more stable refrigeration efficiency, greater attention should be paid to controlling the stability of cold-side heat absorption conditions, material thermal conductance, and thermoelectric figure of merit during engineering applications. However, the parameter perturbations considered in this study were relatively small; these conclusions may change if larger parameter variations are applied. Therefore, future research should consider evaluating the effects of larger changes in these input parameter distributions on the fluctuations in the output performance parameters.

Overall, the results of this analysis indicate that the performance of an annular thermoelectric refrigerator is highly sensitive to its material properties and the match between heat absorption and heat dissipation. Therefore, the findings of this study provide a theoretical basis informing the selection of thermoelectric materials, optimization of structural parameters, and matching of operating conditions for thermoelectric refrigerators. The results also demonstrate that the proposed stochastic analysis method can effectively predict the performance of these systems and inform design choices to ensure their reliability.

Author Contributions: Conceptualization, J.M., M.S., X.L. and F.Z.; Methodology, J.M., X.L. and F.Z.; Software, M.S.; Validation, X.L. and F.Z.; Formal analysis, J.M. and M.S.; Investigation, J.M., M.S. and F.Z.; Writing—original draft, J.M., M.S., X.L. and F.Z. All authors have read and agreed to the published version of the manuscript.

Funding: This research received no external funding.

Data Availability Statement: Data are contained within the article.

Conflicts of Interest: The authors declare no conflict of interest.

References

1. Bayendang, N.P.; Kahn, M.T.; Balyan, V. The Question of Thermoelectric Devices Electrical Resistance—A Practical Investigation From a Peltier Effect (Thermoelectric Cooler/Thermoelectric Heater) Perspective. *Heat Transf.* **2026**, *55*, 1770–1779. [CrossRef]
2. Solovev, B.; Khuziakhmetov, B.; Gamisonia, G.; Khazieva, R. Seebeck effect-based energy generation using Peltier modules. In *Proceedings of the 2025 International Ural Conference on Electrical Power Engineering (UralCon)*; IEEE: New York, NY, USA, 2025; pp. 870–874. [CrossRef]
3. Chen, J.; Wang, R.; Ding, R.; Luo, D. Numerical study on the influence of the Peltier effect on the output of thermoelectric generator system. *Zhongnan Daxue Xuebao (Ziran Kexue Ban)/J. Cent. South Univ. (Sci. Technol.)* **2025**, *56*, 771–780. [CrossRef]
4. Sanduleac, I.; Andronic, S.; Balmus, I. Organic Nanostructured Crystals for Thermoelectric Cooling in Medical Applications. *IFMBE Proc.* **2024**, *91*, 88–95. [CrossRef]
5. Mohamed, E.S. Experimental evaluation of the thermoelectric package air conditioning for an automotive interior application. *Int. J. Refrig.* **2025**, *174*, 34–46. [CrossRef]
6. Zhao, J. Performance Optimization Study of Segmented Semiconductor Thermoelectric Conversion Units. Master's Thesis, Huazhong University of Science and Technology, Wuhan, China, 2023. [CrossRef]
7. Ferrario, A.; Boldrini, S.; Miozzo, A.; Fabrizio, M. Temperature dependent iterative model of thermoelectric generator including thermal losses in passive elements. *Appl. Therm. Eng.* **2019**, *150*, 620–627. [CrossRef]
8. Navarro-Peris, E.; Corberan, J.M.; Ancik, Z. Evaluation of the potential recovery of compressor heat losses to enhance the efficiency of refrigeration systems by means of thermoelectric generation. *Appl. Therm. Eng.* **2015**, *89*, 755–762. [CrossRef]
9. Yang, G.; Sang, L.; Yun, F.-F.; Mitchell, D.R.G.; Casillas, G.; Ye, N.; See, K.; Pei, J.; Wang, X.; Li, J.-F.; et al. Significant Enhancement of Thermoelectric Figure of Merit in BiSbTe-Based Composites by Incorporating Carbon Microfiber. *Adv. Funct. Mater.* **2021**, *31*, 2008851. [CrossRef]
10. Kim, S.; Kihoi, S.K.; Kim, H.; Kahiu, J.N.; Lee, H.S. Synergetic effect of Bi and Al co-doping in GeTe-based thermoelectric materials leading to optimized carrier concentration tuning and high ZT. *J. Alloys Compd.* **2024**, *970*, 172574. [CrossRef]
11. Xie, L.; Yang, J.; Liu, Z.; Qu, N.; Dong, X.; Zhu, J.; Shi, W.; Wu, H.; Peng, G.; Guo, F.; et al. Highly efficient thermoelectric cooling performance of ultrafine-grained and nanoporous materials. *Mater. Today* **2023**, *65*, 5–13. [CrossRef]
12. Wang, Q.; Tang, Y.; Miura, A.; Miyazaki, K.; Horita, Z.; Iikubo, S. Improving thermoelectric properties of Bi_2Te_3 by straining under high pressure: Experiment and DFT calculation. *Scr. Mater.* **2024**, *243*, 115991. [CrossRef]

13. Ji, D.; Haile, N.F.; Li, X.; Li, B.; Rezeq, M.; Cantwell, W.; Zheng, L. Band degeneracy and convergence in high performing thermoelectric materials. *Appl. Energy* **2026**, *404*, 127182. [CrossRef]
14. Ali, A.; Shahid, I.; Ahmad, I.; Xiang, L.; Arif, N.; Younis, M.; Zeng, Y.-J. 2D ferroelectric In2SSeTe with low lattice thermal conductivity and high Seebeck coefficient: A promising thermoelectric material. *Chem. Phys. Lett.* **2026**, *884*, 142586. [CrossRef]
15. Liu, H.; Li, G.; Zhao, X.; Ma, X.; Shen, C. Investigation of the impact of the thermoelectric geometry on the cooling performance and thermal—Mechanic characteristics in a thermoelectric cooler. *Energy* **2023**, *267*, 126471. [CrossRef]
16. Gao, Y.; Zhu, S.; Gao, J.; Miao, L.; Xu, F.; Sun, L. Wearable thermoelectric cooler encapsulated with low thermal conductivity filler and honeycomb structure for high cooling effect. *Mater. Today Phys.* **2024**, *46*, 101491. [CrossRef]
17. Zhang, J.; Song, X.; Tie, Y.; Li, C.; Zhao, H. A novel sandwich-structural cooling and heating system with high power, high COP and small size based on thermoelectric cooler. *Energy Convers. Manag.* **2024**, *322*, 119126. [CrossRef]
18. Tsai, Y.-F.; Wei, P.-C.; Tsou, N.-T.; Chao, Y.-C.; Yen, H.-W.; Lin, J.-Y.; Wang, K.-K.; Wu, H.-J. Grand herringbone architecture securing the high thermoelectric performance of GeTe. *Mater. Today Phys.* **2024**, *41*, 101329. [CrossRef]
19. Zhang, F.; Wang, W.; Zhang, J.; Du, R.; Wang, X.; Liu, Z. Global sensitivity analysis and optimization of a multistage thermoelectric generator based on failure probability. *Energy Rep.* **2023**, *10*, 4629–4640. [CrossRef]
20. Zhang, F.; Cheng, L.; Wu, M.; Xu, X.; Wang, P.; Liu, Z. Performance analysis of two-stage thermoelectric generator model based on Latin hypercube sampling. *Energy Convers. Manag.* **2020**, *221*, 113159. [CrossRef]
21. Wang, X.; Zhang, B.; Yang, P.; Gao, Z.; Zhang, F. Global sensitivity analysis and optimization of multi-stage TEG based on random and fuzzy mixed input variables. *Appl. Therm. Eng.* **2024**, *248*, 123212. [CrossRef]
22. Sandoz-Rosado, E.J.; Weinstein, S.J.; Stevens, R.J. On the Thomson effect in thermoelectric power devices. *Int. J. Therm. Sci.* **2013**, *66*, 1–7. [CrossRef]
23. Meng, F.; Chen, L.; Sun, F. A numerical model and comparative investigation of a thermoelectric generator with multi-irreversibilities. *Energy* **2011**, *36*, 3513–3522. [CrossRef]
24. Cai, Y.; Xiang, Z.; Hong, B.; Huang, N.; Zhao, F. Dimensionless analysis and performance evaluation of annular thermoelectric cooler. *Cryog. Supercond.* **2021**, *49*, 70–77. [CrossRef]
25. Shen, Z.-G.; Wu, S.-Y.; Xiao, L. Theoretical analysis on the performance of annular thermoelectric couple. *Energy Convers. Manag.* **2015**, *89*, 244–250. [CrossRef]
26. Hu, Z.; de León, F.; Wang, R.; Li, Y. Effects of Installing Different Types of Cooling Fins on the Cold Side of a Thermoelectric Power Generation Device on the Thermal Efficiency and Exergy Efficiency of Power Cable Surface Waste Heat Recovery. *Micromachines* **2023**, *14*, 1591. [CrossRef]
27. Al-Tahaineh, H. A novel approach and exergy analysis for a concentrated photovoltaic system for thermoelectric absorption cooling. *Clean. Energy* **2025**, *9*, 11–21. [CrossRef]
28. Ma, M.; Yu, J. An analysis on a two-stage cascade thermoelectric cooler for electronics cooling applications. *Int. J. Refrig.* **2014**, *38*, 352–357. [CrossRef]
29. Hakimi, F. Robust Estimation with Latin Hypercube Sampling: A Central Limit Theorem for Z-estimators. *arXiv* **2026**, arXiv:2502.06321. [CrossRef]
30. Boschini, M.; Gerosa, D.; Crespi, A.; Falcone, M. "LHS in LHS": A new expansion strategy for Latin hypercube sampling in simulation design. *SoftwareX* **2025**, *31*, 102294. [CrossRef]
31. Bayar, G.; Hambarci, G. Improving measurement accuracy of indoor positioning system of a Mecanum wheeled mobile robot using Monte Carlo—Latin hypercube sampling based machine learning algorithm. *J. Frankl. Inst.* **2023**, *360*, 13994–14021. [CrossRef]
32. Joy, G.; Huyck, C.; Yang, X.-S. Parameter Tuning of the Firefly Algorithm by Three Tuning Methods: Standard Monte Carlo, Quasi-Monte Carlo and Latin Hypercube Sampling Methods. *arXiv* **2025**, arXiv:2504.18545. [CrossRef]
33. Buljan, I.; Benković, M.; Jurina, T.; Sokač Cvetnić, T.; Valinger, D.; Gajdoš Kljusurić, J.; Jurinjak Tušek, A. Simulation and Local Parametric Sensitivity Analysis of a Computational Model of Fructose Metabolism. *Processes* **2025**, *13*, 125. [CrossRef]

Disclaimer/Publisher's Note: The statements, opinions and data contained in all publications are solely those of the individual author(s) and contributor(s) and not of MDPI and/or the editor(s). MDPI and/or the editor(s) disclaim responsibility for any injury to people or property resulting from any ideas, methods, instructions or products referred to in the content.